Superwide-angle acoustic propagations above the critical angles of the Snell law in liquid–solid superlattice*

Zhang Sai(张 赛)[a], Zhang Yu(张 宇)[a)b)†], and Gao Xiao-Wei(高晓薇)[a)]

[a)] *Key Laboratory of Underwater Acoustic Communication and Marine Information Technology of the Ministry of Education, Xiamen University, Xiamen* 361005, *China*

[b)] *State Key Laboratory of Marine Environmental Science, Xiamen University, Xiamen* 351005, *China*

(Received 1 April 2014; revised manuscript received 6 May 2014; published online 10 October 2014)

In this paper, superwide-angle acoustic propagations above the critical angles of the Snell law in liquid–solid superlattice are investigated. Incident waves above the critical angles of the Snell law usually inevitably induce total reflection. However, incident waves with big oblique angles through the liquid–solid superlattice will produce a superwide angle transmission in a certain frequency range so that total reflection does not occur. Together with the simulation by finite element analysis, theoretical analysis by using transfer matrix method suggests the Bragg scattering of the Lamb waves as the physical mechanism of acoustic wave super-propagation far beyond the critical angle. Incident angle, filling fraction, and material thickness have significant influences on propagation. Superwide-angle propagation phenomenon may have potential applications in nondestructive evaluation of layered structures and controlling of energy flux.

Keywords: superwide-angle, liquid–solid, Bragg scattering, Lamb wave, superlattice

PACS: 43.25.+y, 43.35.+d **DOI:** 10.1088/1674-1056/23/12/124301

1. Introduction

Incident waves impinging on the interface of another medium with an angle large enough will lead to total reflection in optics and acoustics.[1–4] Such a principle has been successfully applied to the design and fabrication of optical fiber and related fields.[1,3] Usually, the Snell law causes waves to be unable to transmit through the material with incident angle above the maximal critical angle. Nevertheless, in some cases, it is expected that the limitation of Snell law can allow the propagation with incident angle above the second critical angles. Considering the significant practice application to lens design, nondestructive evaluation of layered structures, and relative fields,[5,6] it is highly desired to overcome the above limitation for a wide angle propagation. For example, transmitted waves with wide angles will be helpful for designing distortionless optical or acoustic lenses. In acoustics, non-specular reflection of leaky Lamb waves may obtain wide-angle transmission far beyond the critical angle.[7]

In recent years, phononic crystals and acoustic metamaterials have received widespread attention.[8–24] New acoustic phenomena and transmission disciplines based on special artificial structures and materials have been discovered, such as one way transmission,[19–21] acoustic cloaking,[23,24] superlensing effect.[25] Superlattice, as the most easily realizable sonic crystal with dependable filter property, has been widely studied both theoretically and experimentally.[12–18] For instance, liquid–solid superlattice has been successfully used to fabricate an acoustic diode,[19,20] which has received widespread attention. However, the overwhelming majority of the studies focused on the solid-solid composite superlattice or propagation characteristics of vertical incidence.[8,20,21,25,26] In addition, omnidirectional incident propagation characteristics of liquid–solid superlattice and its band structure have not been thoroughly analyzed. Given the fact that incident acoustic waves can transmit through a plate with a wide angle in the form of Lamb waves according to Snell–Descartes law,[7,27,28] and liquid–solid structure has many advantages in practice, such as its tunable and easy-to-fabricate properties, we may realize super-wide angle propagation by utilizing the scattering properties of leaky Lamb waves in liquid–solid superlattice. Motivated by this, we investigate the omnidirectional propagation of acoustics waves through liquid–solid superlattice and explore the superwide-angle propagation phenomenon in this specific system.

In this paper, we present numerical evidence of the superwide-angle acoustic wave propagations in a liquid–solid superlattice at an arbitrary incident angle based on the transfer matrix method.[29,30] The existence of the superwide-angle acoustic propagation in the superlattice is demonstrated in a certain frequency range and at different ratios of the solid thickness to the lattice spacing. The angles of superwide propagation calculated by transfer matrix method are in good agreement with the results by the finite element method. The influence of the filling fraction on the formation of superwide-angle propagation is discussed in the transmission spectrum.

*Project supported by the National Natural Science Foundation of China (Grant Nos. 41276040 and 11174240) and the Natural Science Foundation of Fujian Province, China (Grant No. 2012J06010).

†Corresponding author. E-mail: yuzhang@xum.edu.cn

© 2014 Chinese Physical Society and IOP Publishing Ltd

The rest of this paper is organized as follows. In Section 2, the phenomenon of the superwide-angle acoustic propagation in liquid–solid superlattice is presented by employing finite element method. In Section 3, the transfer matrix of the liquid–solid superlattice for plane waves with arbitrary oblique incident angles is derived and compared with finite element simulation. In Section 4, numerical results and discussion are given. Finally, in Section 5 some conclusions are drawn from the present study

2. Superwide-angle propagation phenomenon by finite element method

To expound the superwide-angle acoustic propagation in liquid–solid superlattice, finite element method simulations are performed for a linear source with the frequency 376.5 kHz, and oblique incident angle $\theta = 25°$, $\theta = 36.161°$, and $\theta = 63.876°$. The initial pressure wave on one side of liquid will be converted into longitudinal and transverse waves in the solid, and finally converted into longitudinal pressure wave in the liquid on the other side. Figures 1(a)–1(c) compare the pressure distributions of the uniform solid material with those of the liquid–solid superlattice with the same length $L = 56$ mm but different incident angles, where water is set as the background medium I with density $\rho_{\rm I} = 998$ kg/m^3 and longitudinal wave velocity $c_{\rm IL} = 1483$ m/s, and the glass is set as medium II with density $\rho_{\rm II} = 2700$ kg/m^3, longitudinal wave velocity $c_{\rm IIL} = 5570$ m/s, and transverse wave velocity $c_{\rm IIT} = 3520$ m/s. For a uniform solid material, when θ is larger than the first and second critical angles θ_1 and θ_2, total reflection occurs where θ_1 and θ_2 satisfy $\theta_1 = \arcsin(c_{\rm IL}/c_{\rm IIL}) \approx 15.4°$ and $\theta_2 = \arcsin(c_{\rm IL}/c_{\rm IIT}) \approx 24.9°$ according to the Snell law. The acoustic wave cannot propagate through the solid material and thus be unable to be detected on the other side as shown in Fig. 1(a). Total reflection restricts the detection scope of this kind of solid material lens when the incident angle is bigger than θ_2. However, when the liquid–solid superlattice is applied, a wide angle acoustic plane wave which is much larger than the second critical angle θ_2 can propagate though the superlattice as shown in Fig. 1(b), where the superlattice consists of $N = 7$ repetition of alternating layers of water I with thickness $d_{\rm I} = 4$ mm and glass II with thickness $d_{\rm II} = 4$ mm, lattice spacing $D = d_{\rm I} + d_{\rm II} = 8$ mm, and the filling fraction $f_{\rm c} = d_{\rm II}/D = 0.5$. Strong pressure distribution and high transmission both indicate that the high acoustic energy can be easily detected on the other side of the superlattice. In particular, it is found that the maximal oblique incident angle for high transmission is 63.876°, which is almost 2.56 times larger than the second critical angle as shown in Fig. 1(c). Thus, the liquid–solid superlattice breaks down the total reflection limitation of the solid material by significantly increasing oblique incident angle, suggesting its application in superwide-angle lens. The incident angles in both Fig. 1(b) and Fig. 1(c) are larger than the second critical angle, however, the difference is that the wave in Fig. 1(b) is the leaky Lamb wave A_0 mode while the wave in Fig. 1(c) is not. The research[25,26] of acoustic bandgap formation in a periodic structure with multilayer unit cells suggested that narrow pass bands could be obtained when the unit cell has more than two sublayers. Acoustic bandgaps produced by periodic structures originate from multiple reflections at the interface due to the impedance mismatch between the adjacent materials. Thus, we speculate that the Bragg scattering of the superlattice may also produce some new pass bands at oblique incidence situations as shown in Fig. 1(c) which can realize superwide-angle propagation and we will discuss it in detail in Section 4.

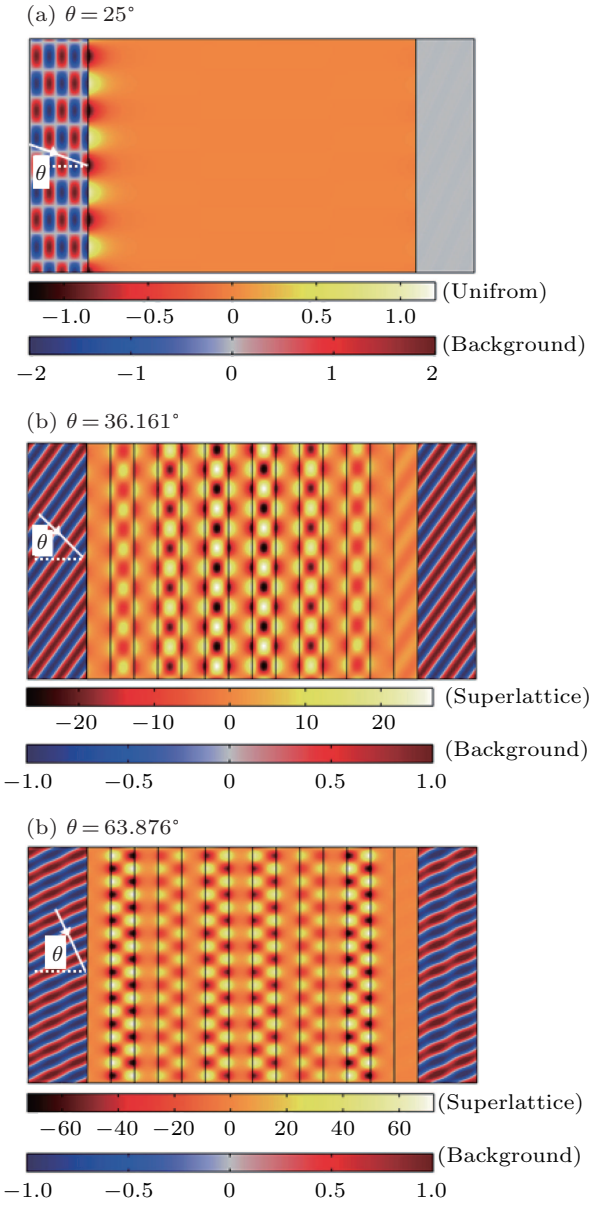


Fig. 1. (color online) Simulated acoustic pressure field distributions at 376.5 kHz. Panel (a) is for uniform solid material with oblique incident $\theta = 25°$, panel (b) for superlattice with oblique incident $\theta = 36.161°$, and panel (c) for superlattice with oblique incident $\theta = 62.876°$ respectively. The rainbow and thermal bars represent pressure field distributions in the background material and superlattice respectively.

3. Formulations

To investigate the principle of the superwide-angle propagation in the liquid–solid superlattice (SL), we used the transfer matrix method for plane waves. Figure 2 depicts the superlattice system, where the x and z axes are normal and parallel to the interfaces, respectively, and a plane longitudinal wave propagates from the left side through the N liquid–solid layers and travels to the right side.

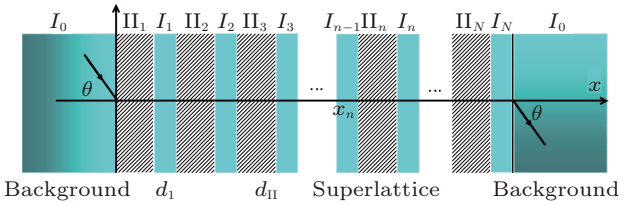


Fig. 2. (color online) Superlattice consisting of alternate glass and water, immersed in water. The symbols I_n , II_n $(1 \le n \le N)$ denote the water and glass layer; $d_{\rm I}$ and $d_{\rm II}$ represent their thickness. The arrows show the directions of the incident and transmission plane waves respectively. θ is the oblique incident angle with respect to the x axis.

In homogeneous linear elastic medium with no body force, the equation of motion for displacement vector $\boldsymbol{v}$ can be written as

$$\rho\frac{\partial^2\boldsymbol{v}}{\partial t^2} = (\lambda+2\mu)\mathrm{grad}(\mathrm{div}\boldsymbol{v}) - \mu\mathrm{rot}(\mathrm{rot}\boldsymbol{v}), \tag{1}$$

where the terms λ and μ are the first and second Lame constants, respectively. When $\mu = 0$, equation (1) can be reduced to the acoustic wave equation in liquid. The displacement field $\boldsymbol{v}$ can be separated into scalar and vector potentials: $v = \mathrm{grad}\Phi + \mathrm{rot}\Psi$ and $\mathrm{div}\Psi = 0$. For the n-th SL layer, the longitudinal wave with Φ_1 passes through the liquid–solid interface at x_n and is converted into the longitudinal Φ_2 and transverse Ψ_2 waves in the solid. The waves are converted back into the longitudinal pressure wave Φ_3 through the liquid–solid interface at $x_n + d_{\rm I}$ in the liquid and then propagate into Φ_4 at $x_{n+1} = x_n + d_{\rm I} + d_{\rm II}$. From the wave equations, by omitting the time factor $\mathrm{e}^{\mathrm{j}\omega t}$, these scalar and vector potentials can be obtained as

$$\begin{aligned}
\Phi_1 &= \Phi_{1i}\mathrm{e}^{-\mathrm{j}(k_{\rm IL}\cos\theta_{\rm IL}x + k_{\rm IL}\sin\theta_{\rm IL}z)} \\
&\quad + \Phi_{1r}\mathrm{e}^{-\mathrm{j}(-k_{\rm IL}\cos\theta_{\rm IL}x + k_{\rm IL}\sin\theta_{\rm IL}z)}, && \text{(2a)} \\
\Phi_2 &= \Phi_{2i}\mathrm{e}^{-\mathrm{j}(k_{\rm IIL}\cos\theta_{\rm IIL}x + k_{\rm IIL}\sin\theta_{\rm IIL}z)} \\
&\quad + \Phi_{2r}\mathrm{e}^{-\mathrm{j}(-k_{\rm IIL}\cos\theta_{\rm IIL}x + k_{\rm IIL}\sin\theta_{\rm IIL}z)}, && \text{(2b)} \\
\Psi_2 &= \Psi_{2i}\mathrm{e}^{-\mathrm{j}(k_{\rm IIT}\cos\theta_{\rm IIT}x + k_{\rm IIT}\sin\theta_{\rm IIT}z)} \\
&\quad + \Psi_{2r}\mathrm{e}^{-\mathrm{j}(-k_{\rm IIT}\cos\theta_{\rm IIT}x + k_{\rm IIT}\sin\theta_{\rm IIT}z)}, && \text{(2c)} \\
\Phi_3 &= \Phi_{3i}\mathrm{e}^{-\mathrm{j}(k_{\rm IL}\cos q\theta(x-d_{\rm II}) + k_{\rm IL}\sin\theta_{\rm IL}z)} \\
&\quad + \Phi_{3r}\mathrm{e}^{-\mathrm{j}(-k_{\rm IL}\cos\theta_{\rm IL}(x-d_{\rm II}) + k_{\rm IL}\sin\theta_{\rm IL}z)}, && \text{(2d)} \\
\Phi_4 &= \Phi_{4i} + \Phi_{4r} \\
&= \Phi_{3i}\mathrm{e}^{-\mathrm{j}k_{\rm IL}\cos\theta_{\rm IL}d_{\rm I}} + \Phi_{3r}\mathrm{e}^{\mathrm{j}k_{\rm IL}\cos\theta_{\rm IL}d_{\rm I}}, && \text{(2e)}
\end{aligned}$$

where $k_{\rm IL}$, $k_{\rm IIL}$, and $k_{\rm IIT}$ denote the longitudinal wave number in the liquid, the longitudinal wave number in the solid, and the transverse wave number in the solid, respectively, and $\theta_{\rm IL}$, $\theta_{\rm IIL}$, and $\theta_{\rm IIT}$ refer to the corresponding oblique incident angles. Φ_{1i}, Φ_{2i}, Φ_{3i}, and Ψ_{2i} represent the transmitted wave amplitudes, while Φ_{1r}, Φ_{2r}, Φ_{3r}, and Ψ_{2r} denote the reflected wave amplitudes.

The boundary conditions of the continuous normal velocity and the balance between the stresses at the interface at x_n satisfy

$$\left.\frac{\partial\Phi_1}{\partial x}\right|_{x=x_n} = \left.\frac{\partial\Phi_2}{\partial x} - \frac{\partial\Psi_2}{\partial z}\right|_{x=x_n}, \tag{3a}$$

$$S_{1xx}|_{x=x_n} = S_{2xx}|_{x=x_n}, \quad S_{1xz}|_{x=x_n} = S_{2xz}|_{x=x_n}, \tag{3b}$$

where $S_{1xx} = \mathrm{j}\omega\rho_{\rm I}\Phi_1$ and

$$S_{2xx} = \frac{\rho_{\rm II}}{j\omega}\left[-\omega^2\Phi_2 - 2c_{\rm IIT}^2\left(\frac{\partial^2\Psi_2}{\partial x\partial z} + \frac{\partial^2\Phi_2}{\partial z^2}\right)\right]$$

represent the normal stresses in the liquid and in the solid at the interface, respectively. While $S_{1xz} = 0$ and

$$S_{2xz} = \frac{c_{\rm IIT}^2}{j\omega}\left(\frac{\partial^2\Psi_2}{\partial x^2} - \frac{\partial^2\Psi_2}{\partial z^2} + 2\frac{\partial^2\Phi_2}{\partial x\partial z}\right)$$

are the corresponding shear stresses.

Similarly, the boundary conditions of the normal speed continuity and stress balance at the interface $x = x_n + d_{\rm II}$ satisfy

$$\left.\frac{\partial\Phi_3}{\partial x}\right|_{x=x_n+d_{\rm II}} = \left.\frac{\partial\Phi_2}{\partial x} - \frac{\partial\Psi_2}{\partial z}\right|_{x=x_n+d_{\rm II}}, \tag{4a}$$

$$\begin{aligned}
&S_{3xx}|_{x=x_n+d_{\rm II}} = S_{4xx}|_{x=x_n+d_{\rm II}}, \\
&S_{3xz}|_{x=x_n+d_{\rm II}} = S_{4xz}|_{x=x_n+d_{\rm II}},
\end{aligned} \tag{4b}$$

where $S_{3xx} = \mathrm{j}\omega\rho_{\rm I}\Phi_3$ and

$$S_{4xx} = \frac{\rho_{\rm II}}{\mathrm{j}\omega}\left[-\omega^2\Phi_2 - 2c_{\rm IIT}^2\left(\frac{\partial^2\Psi_2}{\partial x\partial z} + \frac{\partial^2\Phi_2}{\partial z^2}\right)\right]$$

represent the normal stresses in the liquid and in the solid at the interface, respectively. While $S_{3xz} = 0$, and

$$S_{4xz} = \frac{c_{\rm IIT}^2}{\mathrm{j}\omega}\left(\frac{\partial^2\Psi_2}{\partial x^2} - \frac{\partial^2\Psi_2}{\partial z^2} + 2\frac{\partial^2\Phi_2}{\partial x\partial z}\right)$$

are the corresponding shear stresses.

According to Eqs. (2a)–(2d) and (3a)–(3d), the following equations can be obtained as

$$\begin{aligned}
&\Phi_{1i}k_{\rm IL}\cos\theta_{\rm IL} - \Phi_{1r}k_{\rm IL}\cos\theta_{\rm IL} \\
&= \Phi_{2i}k_{\rm IIL}\cos\theta_{\rm IIL} - \Phi_{2r}k_{\rm IIL}\cos\theta_{\rm IIL} - \Psi_{2i}k_{\rm IIT}\sin\theta_{\rm IIT} \\
&\quad - \Psi_{2r}k_{\rm IIT}\sin\theta_{\rm IIT}, && \text{(5a)} \\
&\Phi_{1i} + \Phi_{1r} \\
&= \frac{\rho_{\rm II}}{\rho_{\rm I}}(\Phi_{2i}\cos 2\theta_{\rm IIT} + \Phi_{2r}\cos 2\theta_{\rm IIT} \\
&\quad - \Psi_{2i}\sin 2\theta_{\rm IIT} + \Psi_{2r}\sin 2\theta_{\rm IIT}), && \text{(5b)} \\
&\Phi_{2i}k_{\rm IIL}^2\sin 2\theta_{\rm IIL} - \Phi_{2r}k_{\rm IIL}^2\sin 2\theta_{\rm IIL}
\end{aligned}$$

$$+\Psi_{2i}k_{\mathrm{IIT}}^2\cos 2\theta_{\mathrm{IIT}}+\Psi_{2r}k_{\mathrm{IIT}}^2\cos 2\theta_{\mathrm{IIT}}=0, \tag{5c}$$

$$\begin{aligned}&\Phi_{3i}k_{\mathrm{IL}}\cos\theta_{\mathrm{IL}}-\Phi_{3r}k_{\mathrm{IL}}\cos\theta_{\mathrm{IL}}\\ =\;&\Phi_{2i}k_{\mathrm{IIL}}\cos\theta_{\mathrm{IIL}}\,\mathrm{e}^{-\mathrm{j}k_{\mathrm{IIL}}\cos\theta_{\mathrm{IIL}}d_{\mathrm{II}}}\\ &-\Phi_{2r}k_{\mathrm{IIL}}\cos q_{\mathrm{IIL}}\,\mathrm{e}^{\mathrm{j}k_{\mathrm{IIL}}\cos\theta_{\mathrm{IIL}}d_{\mathrm{II}}}\\ &-\Psi_{2i}k_{\mathrm{IIT}}\sin\theta_{\mathrm{IIT}}\,\mathrm{e}^{-\mathrm{j}k_{\mathrm{IIT}}\cos\theta_{\mathrm{IIT}}d_{\mathrm{II}}}\\ &-\Psi_{2r}k_{\mathrm{IIT}}\sin\theta_{2T}\,\mathrm{e}^{\mathrm{j}k_{\mathrm{IIT}}\cos\theta_{\mathrm{IIT}}d_{\mathrm{II}}},\end{aligned} \tag{5d}$$

$$\begin{aligned}&\Phi_{3i}+\Phi_{3r}\\ =\;&\frac{\rho_{\mathrm{II}}}{\rho_{\mathrm{I}}}(\Phi_{2i}\cos 2\theta_{\mathrm{IIT}}\,\mathrm{e}^{-\mathrm{j}k_{\mathrm{IIL}}\cos\theta_{\mathrm{IIL}}d_{\mathrm{II}}}\\ &+\Phi_{2r}\cos 2\theta_{\mathrm{IIT}}\,\mathrm{e}^{\mathrm{j}k_{\mathrm{IIL}}\cos\theta_{\mathrm{IIL}}d_{\mathrm{II}}}\\ &-\Psi_{2i}\sin 2\theta_{\mathrm{IIT}}\,\mathrm{e}^{-\mathrm{j}k_{\mathrm{IIT}}\cos\theta_{\mathrm{IIT}}d_{\mathrm{II}}}\\ &+\Psi_{2r}\sin 2\theta_{\mathrm{IIT}}\,\mathrm{e}^{\mathrm{j}k_{\mathrm{IIT}}\cos\theta_{\mathrm{IIT}}d_{\mathrm{II}}}),\end{aligned} \tag{5e}$$

$$\begin{aligned}&\Phi_{2r}k_{\mathrm{IIL}}^2\sin 2\theta_{\mathrm{IIL}}\,\mathrm{e}^{\mathrm{j}k_{\mathrm{IIL}}\cos\theta_{\mathrm{IIL}}d_{\mathrm{II}}}\\ &-\Phi_{2i}k_{\mathrm{IIL}}^2\sin 2\theta_{\mathrm{IIL}}\,\mathrm{e}^{-\mathrm{j}k_{\mathrm{IIL}}\cos\theta_{\mathrm{IIL}}d_{\mathrm{II}}}\\ =\;&\Psi_{2i}k_{\mathrm{IIT}}^2\cos 2\theta_{\mathrm{IIT}}\,\mathrm{e}^{-\mathrm{j}k_{\mathrm{IIT}}\cos\theta_{\mathrm{IIT}}d_{\mathrm{II}}}\\ &+\Psi_{2r}k_{\mathrm{IIT}}^2\cos 2\theta_{\mathrm{IIT}}\,\mathrm{e}^{\mathrm{j}k_{\mathrm{IIT}}\cos\theta_{\mathrm{IIT}}d_{\mathrm{II}}}.\end{aligned} \tag{5f}$$

From the boundary condition of normal speed continuity, the Snell law can be obtained as

$$k_{\mathrm{IL}}\sin(\theta_{\mathrm{IL}})=k_{\mathrm{IIL}}\sin(\theta_{\mathrm{IIL}})=k_{\mathrm{IIT}}\sin(\theta_{\mathrm{IIT}}). \tag{6}$$

To proceed with the derivations, we define state vectors in the corresponding layer as

$$\begin{aligned}\boldsymbol{\Phi}_{n,1}&=\begin{pmatrix}\Phi_{1i}\\ \Phi_{1r}\end{pmatrix}_n,\quad \boldsymbol{\Phi}_{n,2}=\begin{pmatrix}\Phi_{2i}\\ \Phi_{2r}\end{pmatrix}_n,\\ \boldsymbol{\Phi}_{n,3}&=\begin{pmatrix}\Phi_{3i}\\ \Phi_{3r}\end{pmatrix}_n,\quad \boldsymbol{\Phi}_{n,4}=\begin{pmatrix}\Phi_{4i}\\ \Phi_{4r}\end{pmatrix}_n.\end{aligned} \tag{7}$$

From the boundary conditions of stress balance in the n-thunit, the transfer matrix $\boldsymbol{T}_n$ from $\boldsymbol{\Phi}_{n,1}$ to $\Phi_{n,4}$ can be obtained as

$$\boldsymbol{\Phi}_{n,1}=\boldsymbol{T}_n\boldsymbol{\Phi}_{n,4}, \tag{8}$$

where

$$\begin{aligned}\boldsymbol{T}_n&=\boldsymbol{M}_1^{-1}\boldsymbol{M}_2\boldsymbol{M}_4^{-1}\boldsymbol{M}_3\boldsymbol{U}^{-1},\\ \boldsymbol{M}_1&=\begin{pmatrix}k_{\mathrm{IL}}\cos\theta_{\mathrm{IL}} & -k_{\mathrm{IIL}}\cos\theta_{\mathrm{IIL}}\\ 1 & 1\end{pmatrix},\end{aligned}$$

$$\boldsymbol{M}_2=\begin{pmatrix}k_{\mathrm{IIL}}\cos\theta_{\mathrm{IIL}} & -k_{\mathrm{IIL}}\cos\theta_{\mathrm{IIL}} & -k_{\mathrm{IIT}}\sin\theta_{\mathrm{IIT}} & -k_{\mathrm{IIT}}\sin\theta_{\mathrm{IIT}}\\ \dfrac{\rho_{\mathrm{II}}}{\rho_{\mathrm{I}}}\cos 2\theta_{\mathrm{IIT}} & \dfrac{\rho_{\mathrm{II}}}{\rho_{\mathrm{I}}}\cos 2\theta_{\mathrm{IIT}} & -\dfrac{\rho_{\mathrm{II}}}{\rho_{\mathrm{I}}}\sin 2\theta_{\mathrm{IIT}} & \dfrac{\rho_{\mathrm{II}}}{\rho_{\mathrm{I}}}\sin 2\theta_{\mathrm{IIT}}\end{pmatrix},$$

$$\boldsymbol{M}_3=\begin{pmatrix}k_{\mathrm{IL}}\cos\theta_{\mathrm{IL}} & -k_{\mathrm{IL}}\cos\theta_{\mathrm{IL}}\\ 1 & 1\\ 0 & 0\\ 0 & 0\end{pmatrix},$$

$$\boldsymbol{M}_4=\begin{pmatrix}k_{\mathrm{IIL}}\cos\theta_{\mathrm{IIL}}\,\mathrm{e}^{-\mathrm{j}k_{\mathrm{IIL}}\cos\theta_{\mathrm{IIL}}d_{\mathrm{II}}} & -k_{\mathrm{IIL}}\cos\theta_{\mathrm{IIL}}\,\mathrm{e}^{\mathrm{j}k_{\mathrm{IIL}}\cos\theta_{\mathrm{IIL}}d_{\mathrm{II}}} & -k_{\mathrm{IIT}}\sin\theta_{\mathrm{IIT}}\,\mathrm{e}^{-\mathrm{j}k_{\mathrm{IIT}}\cos\theta_{\mathrm{IIT}}d_{\mathrm{II}}} & -k_{\mathrm{IIL}}\sin\theta_{\mathrm{IIT}}\,\mathrm{e}^{\mathrm{j}k_{\mathrm{IIT}}\cos\theta_{\mathrm{IIT}}d_{\mathrm{II}}}\\ \dfrac{\rho_{\mathrm{II}}}{\rho_{\mathrm{I}}}\cos 2\theta_{\mathrm{IIT}}\,\mathrm{e}^{-\mathrm{j}k_{\mathrm{IIL}}\cos\theta_{\mathrm{IIL}}d_{\mathrm{II}}} & \dfrac{\rho_{\mathrm{II}}}{\rho_{\mathrm{I}}}\cos 2\theta_{\mathrm{IIT}}\,\mathrm{e}^{\mathrm{j}k_{\mathrm{IIL}}\cos\theta_{\mathrm{IIL}}d_{\mathrm{II}}} & -\dfrac{\rho_{\mathrm{II}}}{\rho_{\mathrm{I}}}\sin 2\theta_{\mathrm{IIT}}\,\mathrm{e}^{-\mathrm{j}k_{\mathrm{IIT}}\cos\theta_{\mathrm{IIT}}d_{\mathrm{II}}} & \dfrac{\rho_{\mathrm{II}}}{\rho_{\mathrm{I}}}\sin 2\theta_{\mathrm{IIT}}\,\mathrm{e}^{\mathrm{j}k_{\mathrm{IIT}}\cos\theta_{\mathrm{IIT}}d_{\mathrm{II}}}\\ k_{\mathrm{IIL}}^2\sin 2\theta_{\mathrm{IIL}} & -k_{\mathrm{IIL}}^2\sin 2\theta_{\mathrm{IIL}} & k_{\mathrm{IIT}}^2\cos 2\theta_{\mathrm{IIT}} & k_{\mathrm{IIT}}^2\cos 2\theta_{\mathrm{IIT}}\\ k_{\mathrm{IIL}}^2\sin 2\theta_{\mathrm{IIL}}\,\mathrm{e}^{-\mathrm{j}k_{\mathrm{IIL}}\cos\theta_{\mathrm{IIL}}d_{\mathrm{II}}} & -k_{\mathrm{IIL}}^2\sin 2\theta_{\mathrm{IIL}}\,\mathrm{e}^{\mathrm{j}k_{\mathrm{IIL}}\cos\theta_{\mathrm{IIL}}d_{\mathrm{II}}} & k_{\mathrm{IIT}}^2\cos 2\theta_{\mathrm{IIT}}\,\mathrm{e}^{-\mathrm{j}k_{\mathrm{IIT}}\cos\theta_{\mathrm{IIT}}d_{\mathrm{II}}} & k_{\mathrm{IIT}}^2\cos 2\theta_{\mathrm{IIT}}\,\mathrm{e}^{\mathrm{j}k_{\mathrm{IIT}}\cos\theta_{\mathrm{IIT}}d_{\mathrm{II}}}\end{pmatrix},$$

$$\boldsymbol{U}=\begin{pmatrix}\mathrm{e}^{-\mathrm{j}k_{\mathrm{IL}}\cos\theta_{\mathrm{IL}}d_{\mathrm{I}}} & 0\\ 0 & \mathrm{e}^{\mathrm{j}k_{\mathrm{IL}}\cos\theta_{\mathrm{IL}}d_{\mathrm{I}}}\end{pmatrix}.$$

Therefore, any two state vectors of the liquid layers are related by

$$\boldsymbol{\Phi}_{n_1-1,1}=\boldsymbol{T}_{n_1,n_2}\boldsymbol{\Phi}_{n_2}, \tag{9}$$

where $\boldsymbol{T}_{n_1,n_2}=\boldsymbol{T}_{n_1}\boldsymbol{T}_{n_1+1},\ldots,\boldsymbol{T}_{n_2}, 1\le n_1\le n_2\le N$. The transfer matrix $\boldsymbol{T}_{1,N}$ connects the first and last units of the superlattice system, leading to the relationship between total transmission and reflection rates as

$$\boldsymbol{T}_{1,N}=\begin{pmatrix}\dfrac{1}{t} & \dfrac{r^*}{t^*}\\ \dfrac{r}{t} & \dfrac{1}{t^*}\end{pmatrix}, \tag{10}$$

where t and r are transmission and reflection coefficients, $tr=|t|^2$ and $re=|r|^2$ define the transmission and reflection rates, satisfying $tr+re=1$. Using the above transfer matrix method, we can derive the transmissions at different oblique incident angles.

4. Numerical results and discussion

Figure 3 shows the effects of the incident angle on transmission of the monochromatic plane waves with frequency 376.5 kHz, where the solid line and star correspond to the transmission values calculated by using transfer matrix method and finite element method, respectively. The transmissions of acoustic waves in uniform solid material and the superlattice with the same parameters in Section 3 are shown in

Figs. 3(a) and 3(b), respectively. Significant transmission drop above the oblique incident angle 24.9° is found in the uniform solid [see Fig. 3(a)], indicating the total reflection. However, for the superlattice [see Fig. 3(b)], two angles in ranges of 32.3°–36.3° and 63.75°–64.2° show high efficient transmission above the second critical angle, which has no limitation to total reflection. The calculated results match well with the results obtained using the finite element method, which indicates that our derivation of transfer matrix is valid.

Color-scale representations of transmission as functions of both frequency and incident angle are shown in Figs. 4 and 5 by using the transfer matrix method, where the frequency ranges from 100 kHz to 1.5 MHz, and two dot dashed lines correspond to the first [upper] and second [lower] critical angles. Figure 4(a) displays the transmission of a uniform solid material. There is shown neither band properties nor wave propagation through the material when the incident angle is above 24.9°. All of corresponding incident angles with high transmission lower than the second critical angle indicate the existence of the limitation to the total reflection in the uniform material.

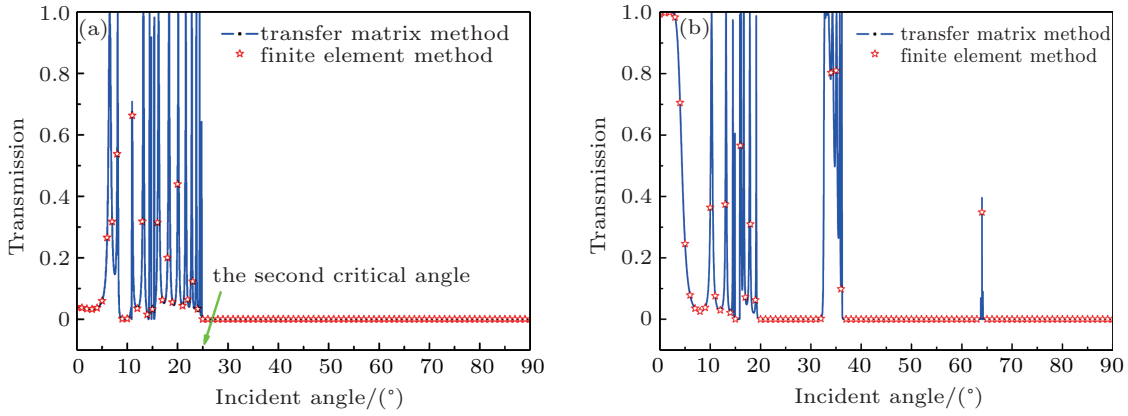


Fig. 3. (color online) Transmissions versus incident angle, calculated by the transfer matrix method and finite element method in (a) the uniform plate and (b) the superlattice with $f_c = 0.5$, $N = 7$, $f = 376.5$ kHz.

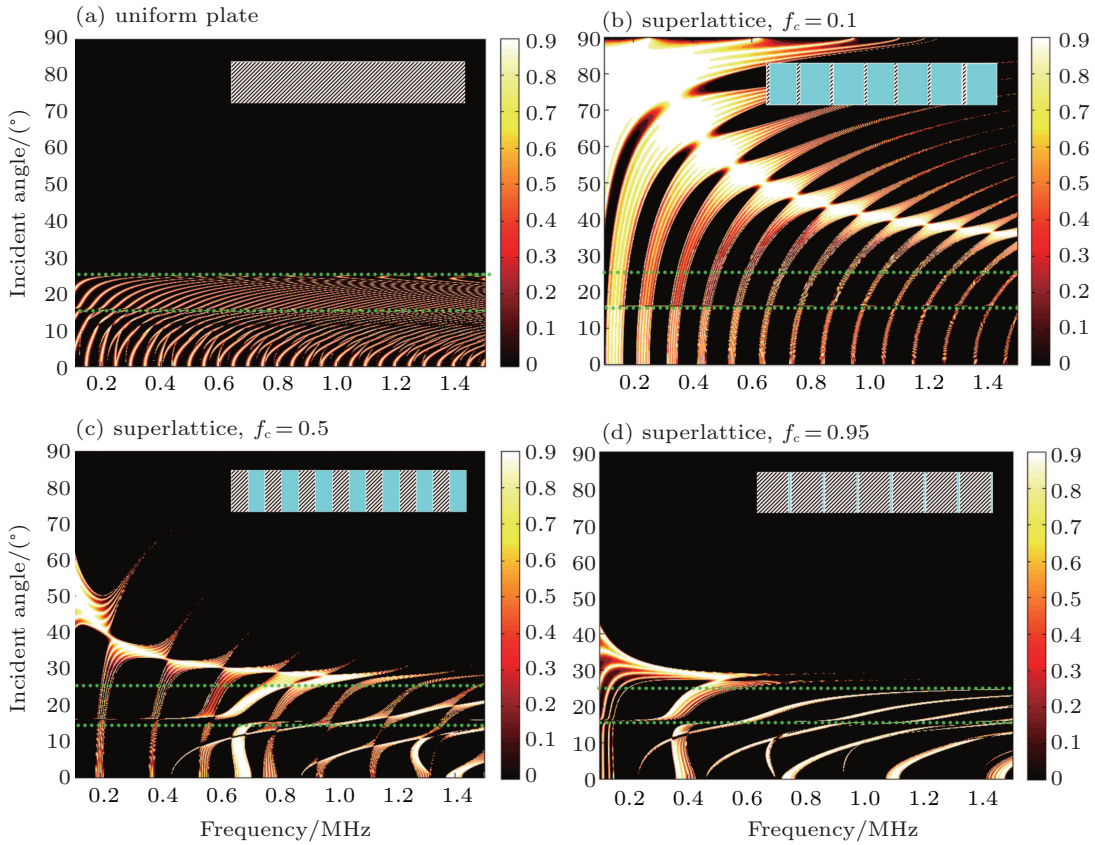


Fig. 4. (color online) Color-scale representations of transmissions as a function of both frequency and incident angle (a) in a uniform plate, and (b)–(d) in a superlattice $N = 7$ with different filling fractions from 0.05 to 0.95. The thermal bar refers to the transmission of the material. The insets show the models of the uniform solid material and the superlattice respectively.

However, in the cases of superlattices with different filling fractions in Figs. 4(b)–4(d), the wide-angle propagation is produced. When the incident angle is zero, corresponding to the vertical incidence, pass and forbidden bands are generated because of Bragg scattering. With the increase of the incident angle, pass bands shifts toward high frequency zones. The Gibbs-type oscillations take place with $(N-1)$ peaks in each pass band. Three filling fractions 0.1, 0.5, and 0.95 are used to investigate the influence of the filling fraction on the transmission by changing the solid thickness of each layer. For the case of $f_c = 0.1$ [Fig. 4(b)], high transmission occurs with large incident angles above 24.9° in each pass band. Besides, it is noteworthy that another region with high transmission overlapping with the pass bands takes place in the region above 35°, which makes the superwide-angle propagation in a wide frequency range in low filling fraction. In this case, the maximum transmission angle can reach 90° at frequency ranging from 0.1 MHz to 1.2 MHz.

When the filling fraction f_c increases to 0.5 as shown in Fig. 4(c), the bandgaps become wider and more Lamb wave modes appear. With the increase of frequency, it becomes more difficult to induce superwide-angle propagation. The maximum transmission angle drops down to 65° within a frequency range of 0.1 MHz–0.42 MHz. When the filling fraction increases to 0.95 [Fig. 4(d)], there are only the A_0 and S_0 modes Lamb waves over the upper line and the maximum angle is much smaller than those of low filling fractions shown in Figs. 4(b) and 4(c). Thus when the filling fraction sufficiently approaches to 1, the superlattice will become a single solid material so that super-propagation mode disappears as shown in Fig. 4(a). In addition, we can see that, the number of Lamb wave modes becomes more with the increase of the filling fraction, while the pattern of A_0mode shifts down and disappears with f_c being bigger than 0.95.

Furthermore, figure 5 shows the effects of solid plate thickness on transmission of the superlattice, where the filling fraction 0.5 is used. Four different superlattices are fabricated with plate thickness values of $L/4$, $L/8$, $L/16$, and $L/32$ as shown in the inset in Figs. 5(a)–5(d). With the decrease of the plate thickness, the bandgaps become wider and the numbers of Lamb wave modes begin to decrease correspondingly, however, the maximum incident angles begin to increase and thus superwide-angle propagation can be more easily obtained. Clearly, the superwide-angle propagation of the liquid–solid superlattice strongly depends on the parameter of the plate thickness and the ratio of the thickness to the lattice spacing. Bragg scattering of Lamb waves, as the physical mechanism of superwide-angle propagation in superlattice, represents a key factor for controlling transmission at oblique incidence. By adjusting the proportion of solid to liquid, superwide-angle propagation can be obtained to break the limitation to the total refraction. The liquid–solid superlattice plays an important role in widening the frequency range and the incident angle of super-wide angle propagation with respect to pure solid material.

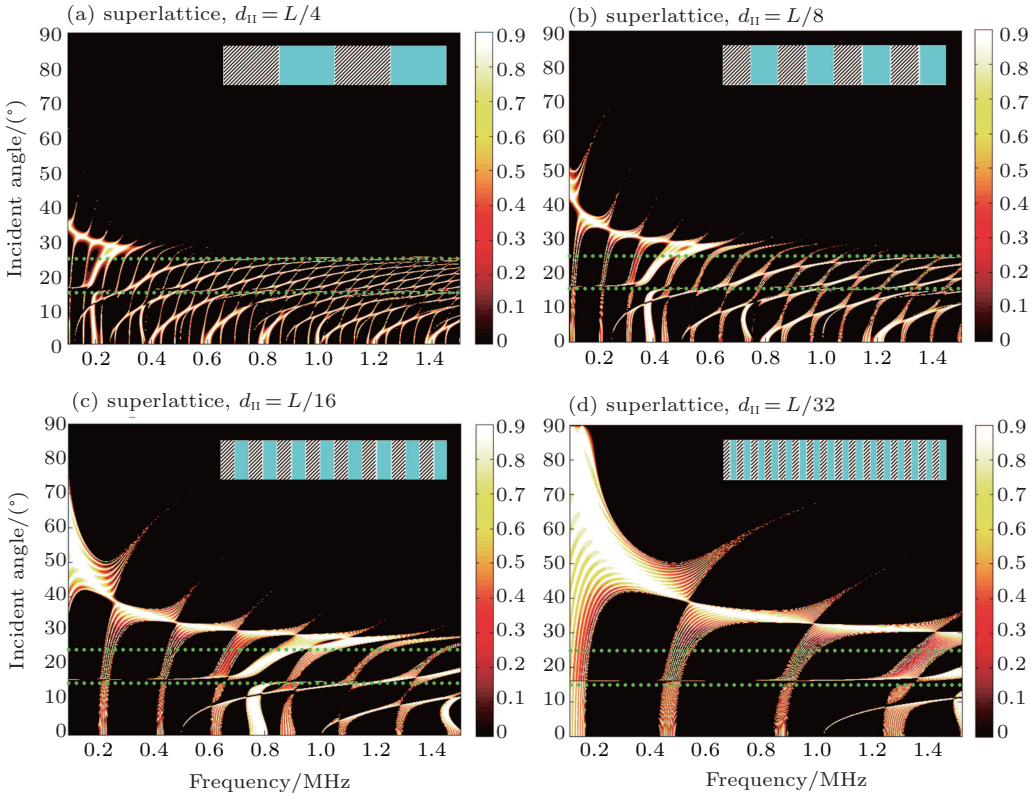


Fig. 5. (color online) Color-scale representations of transmission as a function of both frequency and incident angle in a superlattice with filling fractions 0.5. The thermal bar refers to the transmission of the material.

Figure 6 shows the effects of filling fraction on maximal incident angle for superwide-angle propagation at different frequencies. For low filling fractions, all of the shown frequencies have highly superwide angles close to 90°. However, with the increase of filling fraction, the maximal incident angle decreases rapidly and then becomes close to the second critical angle. It is also found that the sensitivities of the maximal incident angle with different frequencies to the filling fraction are different. High frequency leads to a fast decrease with respect to low frequency, which indicates that at low frequency it is much easier to obtain a high incident angle of superwide-angle propagation.

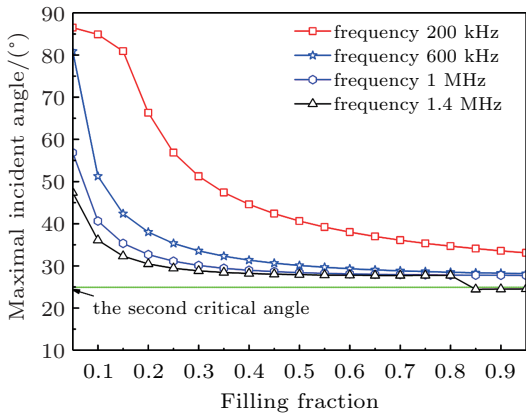


Fig. 6. (color online) Variations of maximal incident angle for superwide-angle propagation with filling fraction at different frequencies.

5. Conclusions

In this paper, the acoustic wave propagation in liquid–solid superlattice with oblique incidence is numerically investigated by using the transfer matrix method and finite element analysis method. The superwide-angle propagation phenomenon above the second critical angle of the Snell law is revealed. It is mainly due to the Bragg scattering of the Lamb waves in the liquid–solid superlattice. Its transmission characteristics have the features of both superlattice and Lamb waves. We also find the significant influences of the filling fraction and thickness on the formation of the superpropagation. The superwide-angle propagation above the second critical angle breaks the limitation to the total refraction, and it may have potential applications in the nondestructive evaluation of layered structures, the controlling of energy flux, and the wide-angle lens design, and in other relevant fields.

Acknowledgment

We thank professor Li Yan (Xiamen University), professor Tang Li-Guo (Xiamen University), for their helpful discussion. And we also thank Song Zhong-Chang (Xiamen University) for his helpful language polishing.

References

[1] Born M and Wolf E 2002 *Principles of Optics*, 7th edn. (expanded) (Cambridge: Cambridge University Press)
[2] Rose J L 1999 *Ultrasonic Waves in Solid Media* (Cambridge: Cambridge University Press)
[3] Snyder A L and Love J D 1983 *Optical Waveguide Theory* (London: Chapman and Hall)
[4] Viktorov I A 1967 *Rayleigh and Lamb Waves* (New York: Plenum)
[5] Su Z Q, Ye L and Lu Y 2006 *J. Sound Vib.* **295** 753
[6] Castaings M and Cawley P 1996 *J. Acoust. Soc. Am.* **100** 3070
[7] Finney W J 1948 *J. Acoust. Soc. Am.* **20** 626
[8] Cai C, Zhu X F, Chen Q,Yuan Y, Liang B and Cheng J C 2011 *Chin. Phys. B* **20** 116301
[9] Gu Z M, Liang B and Cheng J C 2013 *Chin. Phys. B* **22** 014303
[10] Gao X W, Chen S B, Chen J B, Zheng Q H and Yang H 2012 *Chin. Phys. B* **21** 064301
[11] Chen W, Xie Z X and Wei R 1998 *Chin. Phys. Lett.* **15** 813
[12] Huang G, Lou S, Dai X and Yan J 1989 *Chin. Phys. Lett.* **6** 393
[13] Chen Q, Yang X Q, Zhao X Y, Wang Z H and Zhao Y M 2012 *Acta Phys. Sin.* **61** 044501 (in Chinese)
[14] Lü J, Zhao Z Y, Zhang Y N and Zhou C 2010 *Acta Phys. Sin.* **59** 8662 (in Chinese)
[15] Qian Z W, Guo L H and Xiao L 2004 *Chin. Phys.* **13** 1059
[16] Qian Z W 2001 *Chin. Phys.* **10** 636
[17] Zhang C B, Qiu Y Y, Xi X Y and Zhang D 2009 *Acta Phys.Sin.* **58** 3996 (in Chinese)
[18] Cui W C, Tu J, Hwang J H, Li Q, Fan T B, Zhang D, Chen J H and Chen W Z 2012 *Chin. Phys. B* **21** 074301
[19] Zhang C B, Liu Z, Guo X S and Zhang D 2011 *Chin. Phys. B* **20** 024301
[20] Liang B, Guo X S, Tu J, Zhang D and Cheng J C 2010 *Nat. Mater.* **9** 989
[21] Liang B,Yuan B and Cheng J C 2009 *Phys. Rev. Lett.* **103** 104301
[22] Zhang S and Zhang Y 2014 *Chin. Sci. Bull.* **59** 3239
[23] Xu T, Zhu X F, Liang B, Li Y, Zou X Y and Cheng J C 2012 *Appl. Phys. Lett.* **101** 033509
[24] Li J, Fok L,Yin X , Bartal G and Zhang X 2009 *Nat. Mater.* **8** 931
[25] Shen M and Cao W W 2000 *J. Phys. D: Appl. Phys.* **33** 1150
[26] Cao W W and Qi W K 1995 *J. Appl. Phys.* **78** 4627
[27] Nishino H, Masuda S, Yoshida K, Takahashi M, Hoshino H, Ogura Y, Kitagawa H, Kusumoto J and Kanaya A 2008 *Mater. Trans.* **49** 2861
[28] Fay R D and Fortier O V 1951 *J. Acoust. Soc. Am.* **23** 339
[29] Luan P G and Ye Z 2001 *Phys. Rev. E* **63** 066611
[30] Zhang Y, Li Y, Shao H , Zhong Y, Zhang S and Zhao Z 2012 *Phys. Rev. E* **85** 066319